ChemPubSoc Europe

DOI: 10.1002/open.201900190

Open Access ChemistryOPEN Full Papers

One-Step Synthesis of NiFe Layered Double Hydroxide Nanosheet Array/N-Doped Graphite Foam Electrodes for Oxygen Evolution Reactions

Rui Li,[a] Jingsong Xu,[b] Qifa Pan,[b] Jingwen Ba,[a] Tao Tang,[a] and Wenhua Luo*[a]

Developing cost-effective and highly efficient oxygen evolution reaction (OER) electrocatalysts is vital for the production of clean hydrogen by electrocatalytic water splitting. Here, three dimensional nickel-iron layered double hydroxide (NiFe LDH) nanosheet arrays are in-situ fabricated on self-supporting nitrogen doped graphited foam (NGF) via a one-step hydrothermal process under an optimized amount of urea. The as prepared NiFe LDH/NGF electrode exhibits a remarkable activity toward OER with a low onset overpotential of 233 mV and a Tafel slope of 59.4 mV dec^{-1} as well as a long-term durability. Such good performance is attributed to the synergy among the doping effect, the binder-free characteristic, and the architecture of the nanosheet array.

1. Introduction

Oxygen evolution reaction (OER) is regarded as the largest obstacle for clean hydrogen production by electrochemical water splitting because large overpotentials are generally required ascribed to the sluggish kinetics.[1–4] To improve the OER kinetics, precious metal oxides such as IrO_2 and RuO_2 have been investigated as the most active catalysts.[5,6] However, their practical applications are impeded by their high costs and poor durability.[7] Consequently, it is urgent to develop non-precious metals or earth-abundant elements based electrocatalysts requiring relatively low overpotentials to initiate OER.[8–12] As reported, low-cost transition metals and their derivatives, especially Ni based oxides,[13,14] hydroxides,[15,16] sulfides,[17–19] and phosphides[20,21] have been indicated as favorable candidates for water splitting because of their earth abundance and high catalytic performance characteristics. Among these candidates, NiFe layered double hydroxide (LDH) catalysts have been attracting more and more research attention in electrocatalysis because of their special nanostructure, tunable composition, and large specific surface area.[22–27] To improve the intrinsic conductivity, LDH coupled with carbonaceous materials (graphene, carbon nanotubes, and carbon quantum dots etc.) has been widely explored.[28–31] Moreover, the introduction of nitrogen dopants in these nanocarbons has been demonstrated as an efficient mean to further improve the dispersion of LDHs and the charge transfer because of the created anchoring sites and enhanced electron-donor property, respectively.[32–35]

The mass transport and diffusion issue during OER should also be considered since it occurs at the triple-phase boundary regions.[36–38] To enhance the diffusion of liquid reactants and gas products, directly fabricating the active species with three dimensional (3D) architecture on free-standing conductive substrates as integrated electrodes has been explored.[39–42] Concomitantly, the active sites are adequately exposed by constructing 3D nanostructures;[43–46] the electrochemically active surface area, penetration of electrolyte, and transportation of electron are also increased by the binder-free characteristic.[47] Considering these aforementioned factors, it would be of substantial significance to develop a facile and efficient strategy for loading NiFe LDHs with 3D architectures on a free-standing nitrogen-doped substrate for OER.

Herein, we report a one-step hydrothermal method to facilely fabricate vertically aligned NiFe LDH nanosheet arrays on free-standing nitrogen doped graphite foams (NGF) under an appropriate amount of urea as a hybrid OER electrode (NiFe LDH/NGF). The urea content was optimized to provide the proper condition for simultaneously growing aligned LDH nanosheets and introducing nitrogen dopants into graphite foam, which synergistically benefit the electrocatalytic performance. As expected, this optimized free-standing NiFe LDH/NGF electrocatalyst exhibited a superior OER performance with a low onset overpotential of 0.233 V and Tafel slope of 59.4 mV dec^{-1}, respectively. This work provides a detailed elucidation about the effect of urea content on the formation of LDH and N doping in the suppport, which would benefit the preparation of other metal based LDH electrocatalysts.

[a] R. Li, J. Ba, Prof. Dr. T. Tang, Prof. Dr. W. Luo
Insitute of Materials
China Academy of Engineering Physics
Jiangyou, 621907, China
E-mail: luowenhua@caep.cn
[b] J. Xu, Dr. Q. Pan
Science and Technology on Surface Physics and Chemistry Laboratory
Jiangyou, 621908, China

Supporting information for this article is available on the WWW under https://doi.org/10.1002/open.201900190

2. Results and Discussion

2.1. Morphology and Structure of the Electrodes

NiFe LDH/NGF electrodes were prepared by a facile one-step hydrothermal method. The precursor substrate, commercial graphite foil (GFL), composed of tensely stacked graphite sheets with a thickness of ~100 μm (Figure S1) were firstly oxidized by mixed acids to obtain oxidized graphite foam (OGF) with a much rougher surface and larger thickness (~600 μm) (Figure S2). Then, the reduction of OGF, the doping of N elements and the in-situ growth of NiFe LDH sheets concurrently happened during the hydrothermal process and NiFe LDH/NGF electrodes (~500 μm in thickness) were obtained (Figure S3). Notably, NiFe LDH/NGF electrodes exhibited different morphologies and structures when adjusting the ratio of concentration of urea (C_{urea}) to that of metal ions (C_M) (Figure 1, Figures S4 and S5). In the case of the as-obtained NiFe LDH/NGF-1 (C_{urea}/C_M = 1.0), NiFe LDH sheets tended to aggregate together and stack disorderly on the substrate (Figure 1a,b,S4). This phenomenon is resulted from the insufficient anchoring sites of N dopants for NiFe LDH sheets. With a higher concentration ratio, NiFe LDH/NGF-2 exhibited more uniform structure and the aggregation of LDH sheets were greatly suppressed (Figure S5). When C_{urea} reached 0.2 M, 3D LDH nanosheets with a thickness of about 20 nm almost vertically grew on NGF in NiFe LDH/NGF-4 (Figure 1c, d), which may facilitate the rapid diffusion of O_2 bubbles yielded in catalysis process.[48] The corresponding energy dispersive X-ray spectroscopy (EDS) mapping images further verify the homogeneous dispersion of Ni, Fe, C, O and N elements (Figure S6). However, the nanosheet-array structures of LDH sheets were destructed once the concentration of urea rose to a very high level. Small amorphous particles and cubic particles then appeared on the surface of NiFe LDH/NGF-10 and NiFe LDH/NGF-20, respectively (Figure S7 and Figure 1e, f). Therefore, the concentration ratio of C_{urea}/C_M should be precisely controlled to fabricate LDH sheets with desired structure.

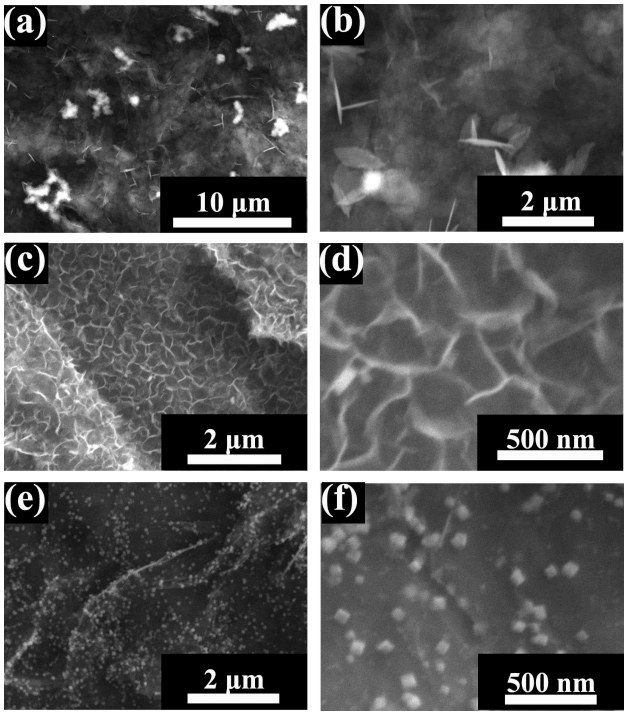

Figure 1. Top-view SEM images of the (a, b) NiFe LDH/NGF-1 electrode, (c, d) NiFe LDH/NGF-4 electrode, and (e, f) NiFe LDH/NGF-20 electrode.

To further investigate the composition of above samples, X-ray photoelectron spectra (XPS) were carried out. The survey spectrum of NiFe LDH/NGF-4 in Figure 2a confirms the existence of Ni, Fe, C, O, and N elements in the hybrid material without any other impurities. The high-resolution C1s core-level spectrum exhibits two fitted peaks corresponding to C=C/C–C (284.5 eV) and C–O (286.4 eV), respectively (Figure 2b). A much larger peak of C=C/C–C than C–O implies the almost integrated graphitic domains of NGF-4 substrates.[49] For NGF, XPS survey also showed the existence of C, O, and N elements (Figure S8a). The C=C/C–C peak of NiFe LDH/NGF-4 was slightly broader than that of NGF because the further reduction of the substrate was hindered by the covered LDHs. By comparing the high-resolution O 1s XPS spectra, it was found that C–O and C=O species existed in both NiFe LDH/NGF-4 and NGF substrates (534.6 eV and 532.6 eV), while Ni–OH showed a large peak in NiFe LDH/NGF-4 (Figure 2c and S8c). The high-resolution N 1s XPS spectra of NiFe LDH/NGF-4 showed the existence of N, mainly in pyrrolic N and graphitic N forms, in consistence with that in NGF (1.64% N atom in NGF) (Figure 2d and S8d).[50,51] In addition, negligible N peak was observed in NiFe LDH/NGF-1 sample and a larger one was observed in NiFe LDH/NGF-20, indicating that N doping occured when urea was sufficiently provided (Figure S9 and S10). Figure 2e shows the Ni $2p_{3/2}$ high resolution spectra of NiFe LDH/NGF-1, 4 and 20. NiFe LDH/NGF-4 showed a higher Ni amount than NiFe LDH/NGF-1, while NiFe LDH/NGF-20 showed an almost negligible amount of Ni element. This is because that when the production of NH_3 is insufficient and thereby the low alkalinity is disadvantageous for forming LDH sheets in NiFe LDH/NGF-1. However, when NH_3 is excessive, $Ni(OH)_2$ converts to $Ni(NH_3)_6^{2+}$ and returns to the solution, leading to a collapse of LDH structure. Moreover, the peak of Ni $2p_{3/2}$ shifted to higher binding energy in NiFe LDH/

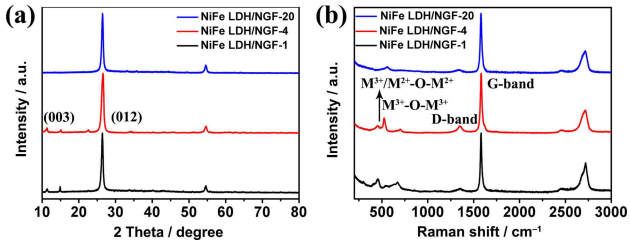

Figure 2. (a) XPS survey, (b) C1s, (c) O 1s, and (d) N 1s high-resolution XPS spectra and corresponding fitting spectra of NiFe LDH/NGF-4 electrode; (e) Ni $2p_{3/2}$ and (f) Fe $2p_{3/2}$ high resolution XPS spectra of NiFe LDH/NGF-1, NiFe LDH/NGF-4, and NiFe LDH/NGF-20 electrodes.

NGF-4 than that of NiFe LDH/NGF-1. The shifted peak position reveals an changed electronic structure of Ni cations, which is because the C–N…Ni–O band becomes stronger when more N elements are doped.[35] The strong binding between NiFe LDH and NGF has profound influence on OER process by tuning the redox behavior of Ni cations and facilitating a rapid charge transfer.[51] While Fe $2p_{3/2}$ peaks of NiFe LDH/NGF-1, 4 and 20 indicate that the amount of Fe increased with the addition of urea because the increased pH facilitated the deposition of Fe $(OH)_3$ on the substrate (Figure 2f).

On the basis of aforementioned SEM and XPS results, the hydrothermal process is illustrated as follows. To begin with, urea slowly decomposed to NH_3 and CO_2 at high temperature. A part of the released NH_3 would hydrolyze to provide the necessary alkaline environment with the release of NH_4^+ and OH^- ions; the other part would selectively dope into OGF or coordinate to Ni^{2+} ions according to the remaining amount. Since the double hydrolysis process is fast and irreversible, only hydrolysis occurred when urea was insufficient. As a result, negligible N doping appeared in NiFe LDH/NGF-1, which could not provide enough N dopants to interact with active species, leading to the aggregation of NiFe LDH sheets. With further addition of urea, NH_3 was not consumed off after hydrolysis process, thus allowing considerable N doping. As a result, N element was observed in NiFe LDH/NGF-4, and the ratio of Ni/Fe was calculated to be 3.95, which is consistent with the raw solution and in the optimal composition range for NiFe LDH as OER catalysts.[47,53,54] In addition, NiFe LDH/NGF-4 exhibited relatively uniform nanosheet arrays during the equilibrium of LDH sheets precipitation/dissolution process due to the strong interaction between uniformly dispersed N dopants and LDH sheets. When urea was excessive, more and more NH_3 was produced with the hydrothermal process going on. The extra NH_3 coordinated to Ni^{2+} to form more stable $Ni(NH_3)_6^{2+}$, thus breaking the equilibrium of NiFe LDH sheets precipitation/dissolution. As a result, Ni^{2+} in NiFe LDH dissolved and the LDH sheets structure converted to amorphous and cubic structure in NiFe LDH/NGF-10 and 20 with limited Ni elements residues, respectively. Therefore, for better governing the preparation of NiFe LDH/NGF electrodes, the formation of LDH and doping of OGF during the hydrothermal process should be precisely controlled by adjusting the C_{urea}/C_M ratio. Here, we propose NiFe LDH/NGF-4 as a suitable electrode for OER catalysis.

To gain deeper insight into the structure of NiFe LDH/NGF electrodes, X-ray diffraction (XRD) analysis together with Raman technique were conducted (Figure 3). XRD patterns demonstrate that the deposited NiFe LDH in NiFe LDH/NGF-4 and 1 are well crystallized with peaks at 11.7°, 23.2°, and 33.6°, corresponding to (003), (006) and (012) lattice planes of α-Ni $(OH)_2$ (JCPDS 38-0715), respectively, while negligible LDH is observed in NiFe LDH/NGF-20 (Figure 3a).[37] Raman spectrum of NiFe LDH/NGF shows typical characteristic bands of graphite, a strong G-band at about 1580 cm^{-1} and a D-band at 1330 cm^{-1}, corresponding to the graphitic domains and the structural defects of graphite, respectively (Figure 3b).[55] And the intensity ratio of D and G peak (I_D/I_G) of NiFe LDH/NGF-4 (0.14) indicates a relatively good graphitic structure, in consistence with the

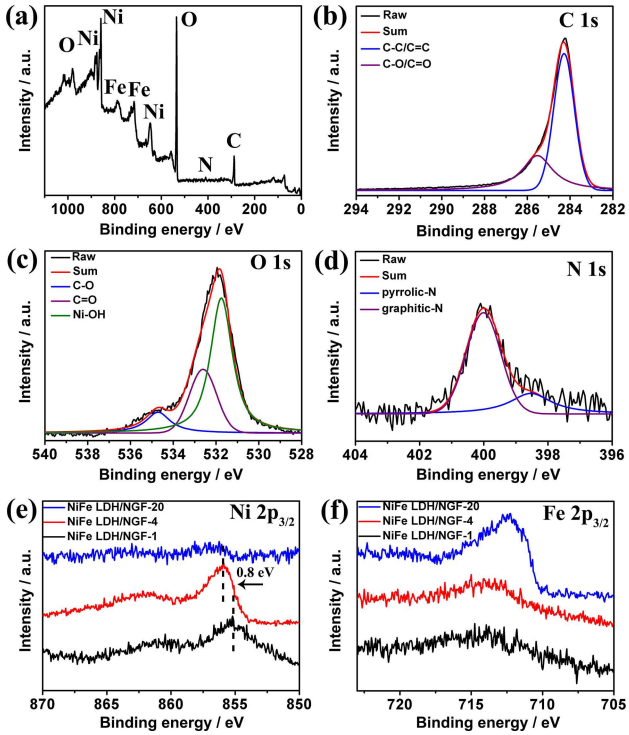

Figure 3. (a) XRD patterns, and (b) Raman spectra of NiFe LDH/NGF-1, NiFe LDH/NGF-4 and NiFe LDH/NGF-20 electrodes.

XPS results. Raman shift at 460 cm^{-1} and 525 cm^{-1} for NiFe LDH/NGF are related to Fe^{3+}/Ni^{2+}–O–Ni^{2+} and Fe^{3+}–O–Fe^{3+} linkage bands, respectively,[35] while Fe^{3+}/Ni^{2+}–O–Ni^{2+} signal is not presented in NiFe LDH/NGF-20, in line with previous discussion about the formation of LDH.

2.2. Electrochemical Performance

The electrocatalytic performance of NiFe LDH/NGF electrodes towards OER was examined in O_2 saturated 1.0 M KOH solution with a standard three-electrode system. For easy comparison, the as prepared NGF and IrO_2/NGF electrodes were also tested under the same condition. Linear sweep voltammetry (LSV) plots were recorded at a scan rate of 10 mV s^{-1} as illustrated in Figure 4a. It is found that NGF substrate exhibits large onset overpotential of 0.368 V, suggesting a weak OER catalytic activity. When coated by NiFe LDH, NiFe LDH/NGF-4 shows a much reduced onset overpotential of 0.233 V, indicating the better OER catalytic activity which is superior to IrO_2/NGF electrode (0.240 V) and the reported NiFe based OER catalysts (Table S1).[23,32,47,56–59] Tafel slopes of NiFe LDH/NGF-4, NGF and IrO_2/NGF electrodes were calculated to be 59.4, 127.5, and 62.5 mV dec^{-1}, respectively, confirming the better catalytic activity of NiFe LDH/NGF-4.

Consistent with the change of morphology and element composition, the catalytic performance of the NiFe LDH/NGF electrodes depends on urea content in hydrothermal process. The LSV curves of NiFe LDH/NGF electrodes show that NiFe

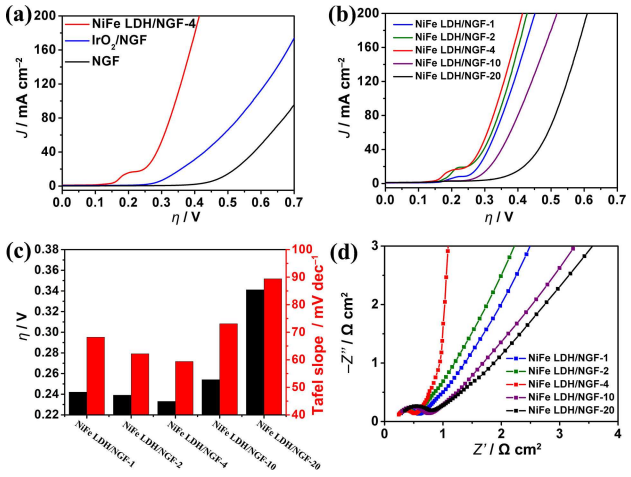

Figure 4. (a) LSV plots of NiFe LDH/NGF-4, IrO_2/NGF, and NGF electrodes in 1.0 M KOH; (b) LSV plots, (c) Onset overpotential and Tafel slopes, and (d) EIS measurements of NiFe LDH/NGF-1, 2, 4, 10, and 20 electrodes.

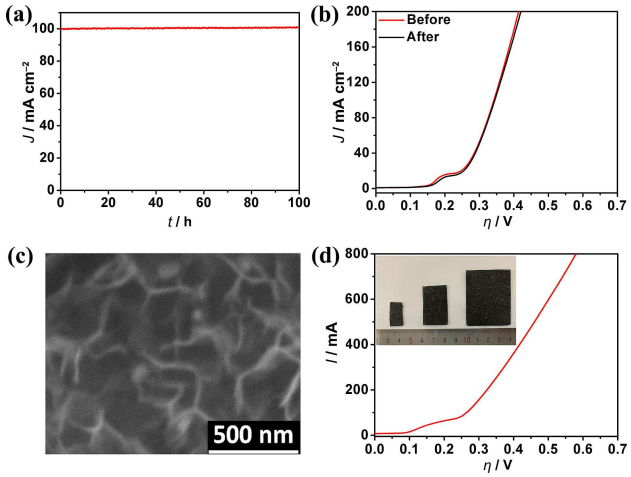

Figure 5. (a) The stability performance of NiFe LDH/NGF-4 electrode; (b) LSV plots of the NiFe LDH/NGF-4 electrode before and after the stability performance tests; (c) SEM image of NiFe LDH/NGF-4 electrode after the stability performance tests; (d) LSV plots of NiFe LDH/NGF-4 (2 cm × 3 cm) electrodes, inset: digital picture of NiFe LDH/NGF-4 with different sizes.

LDH/NGF-4 exhibits the lowest onset potential and tafel slope (Fig 4b, c). In comparison with NiFe LDH/NGF-1 and 2 samples, the superior activity of NiFe LDH/NGF-4 is attributed to the N doping in NGF, which has a significant effect on the electrocatalytic behaviour of NiFe LDH/NGF electrodes. Uniformly dispersed N dopants assist the dispersion of NiFe LDH and the formation of 3D nanosheet-array structures, thus facilitating the diffusion of liquid reactants and gas products. Meanwhile, strong binding between N and Ni cations also shifts the Ni^{2+}/Ni^{3+} redox peak to low potential direction and increased the peak area (peak potential = 0.231, 0.224 and 0.210 V for NiFe LDH/NGF-1, 2 and 4, respectively), suggesting an enhanced transformation between $Ni(OH)_2$ and NiOOH.[35] And it has been approved that NiOOH phase is pivotal to active sites of NiFe LDHs for OER.[60,61] In comparison, the destructed NiFe

LDH structure by excessive urea content shows negligible Ni^{2+}/Ni^{3+} redox peak and much reduced catalytic activity (see NiFe LDH/NGF-10 and 20). We also examined the influence of Ni/Fe ratio on the OER activity, and adopted an optimized Ni/Fe ratio of 4:1 (Figure S11), in consistence with the previous reports.[47,53,54]

The kinetic of the catalytic process on the NiFe LDH/NGF samples were investigated by electrochemical impedance spectra (EIS) measurement at open circuit potential in 1.0 M KOH solution (Figure 4d). All the Nyquist plots of NiFe LDH/NGF catalysts exhibit similar tendency with a semicircle and a straight line, corresponding to the high-frequency region and low-frequency region. The charge transfer resistance (R_{ct}) related to the electrocatalytic kinetics was determined on the basis of the diameter of the semicircle. Obviously, the NiFe LDH/NGF-4 exhibits the smallest diameter, which is calculated to be 0.24 Ω cm^2 (0.26, 0.29, 0.41, 0.47 Ω cm^2 for NiFe LDH/NGF-1, 2, 10, and 20, respectively), implying high charge transport efficiency. This enhanced kinetic should be ascribed to the strong interaction between N dopants and NiFe LDH nanosheets, the highly conductive self-supporting substrate without other additives, and the accelerated diffusion of electrolyte and gas bubbles.[39,47]

The electrochemical stability is another vital parameter to evaluate its OER performance. Figure 5a reveals that the current density still remained about 100 mA cm^{-2} over 100 h of continuous electrolysis at 1.57 V (vs. RHE). The almost overlapped LSV curves and well-reserved porous morphology of NiFe LDH/NGF-4 electrode (Figure 5b, c and Figure S12) obtained after electrolysis further verified its excellent durability and physical stability. This enhanced durability of NiFe LDH/NGF-4 electrocatalyst was attributed to the strong binding energy between N dopants and NiFe LDH sheets, and the facilitated gas releasing. Additionally, this one-step hydrothermal method can be scaled up to produce larger electrodes with different sizes (Figure 5d). For example, a NiFe LDH/NGF-4 electrode with a size of 2 cm × 3 cm showed a similar onset potential but a larger current.

3. Conclusions

In summary, we have grown vertically aligned NiFe LDH nanosheet arrays on free-standing NGF for OER via a one-step hydrothermal process with the optimized amount of urea. The hybrid NiFe LDH/NGF-4 electrode exhibited a small onset overpotential of 0.233 V with long-term durability in alkaline electrolyte. The superior electrochemical performance could be ascribed to the 3D nanostructure together with binder-free characteristic that provide adequate electrochemical active sites and facilitate the transportation of electrolyte and gas products, and the doping effects that enhances the intrinsic activity of NiFe LDH and accelerates the electron transfer. The above results not only elucidate the role of urea in the hydrothermal process but also pave the way to the development of other

metal based LDH with well-designed nanostructures for application in electrocatalysis.

Experimental Section

Pretreatment of GFL

A commercial GFL (Beijing Jingtan Inc, 100 μm in thickness) was firstly cut into small pieces (0.5 cm × 1.0 cm). And then those sheets were treated with a mixed acid solution (65 wt% HNO_3 : 98 wt% H_2SO_4 = 3 : 1) for 12 h at room temperature.[62] The as-obtained OGF sheets were dialyzed with copious water till the solution is neutral.

Synthesis of NiFe LDH/NGF Electrode

NiFe LDH/NGF electrodes were prepared by a facile one-step hydrothermal method. In a typical synthesis process, OGF sheets were put into a Teflonlined autoclave containing 0.04 M $NiSO_4$, 0.005 M $Fe_2(SO_4)_3$, and different concentration of urea for a hydrothermal reaction at 180 °C for 12 h. The concentration of urea was 0.05 M, 0.1 M, 0.2 M, 0.5 M, and 1 M, and the as-prepared electrodes were denoted in terms of the ratio C_{urea} to C_M (e.g., NiFe LDH/NGF-4 corresponds to C_{urea} is 0.2 M and $C_{urea}:C_M = 4:1$). Successively, the as-prepared NiFe LDH/NGF electrodes were immersed in deionized water to remove residual impurities. The mass loading of NiFe LDH/NGF-1, 2, 4, 10 and 20 were measured to be 1.0, 1.1, 1.1, 0.7 and 0.3 mg cm^{-2}. As a comparison, NGF was prepared with a similar hydrothermal method with 0.2 M urea except the addition of metal salts. NiFe LDH/NGF-4 electrodes with other Ni/Fe ratio (5:0, 3:2, 2:3, 1:4, 0:5) were fabricated via a similar hydrothermal method with a total amount of metal ions of 0.05 M.

Characterization

Scanning electron microscopy (SEM) images were obtained from a field emission Siron-200 SEM (FEI Inc) at 10 kV. XPS analyses were recorded on a PHI 5000 XPS system with an Al Ka X-ray source (1486.6 eV photons). XRD patterns were obtained on a Y-2000 X-ray diffractometer with Cu Kα radiation (λ = 0.15418 nm, Dandong Aolong Instruments). Raman tests were performed on an Almega XR Raman microscope with a 532 nm laser, and the power irradiating the sample was 1 mW.

Electrochemical Tests

Electrochemical performance was tested in a standard three-electrode system on a CHI 760D electrochemical workstation (CH Instrument Inc.). NiFe LDH/NGF, platinum mesh and Hg/HgO electrodes were used as the working electrode, counter electrode and reference electrode, respectively. Linear sweep voltammetry (LSV) tests and Tafel plots are performed in O_2 saturated 1.0 M KOH solution with a scan rate of 10 mV s^{-1} without iR correction. EIS tests were measured in the frequency range from 100 kHz to 1.0 Hz with an AC amplitude of 5 mV and the initial potential was the corresponding open circuit potential. The durability studies of the NiFe LDH/NGF electrode were performed in 1.0 M KOH by a long term electrochemical electrolysis at 1.57 V (vs. RHE) for 100 h. In comparison with NiFe LDH/NGF electrodes, IrO_2 catalyst was also loaded on NGF as follows: 20 mg IrO_2 and 50 μL Nafion solution were dispersed in 950 μL ethanol with sonication for 30 min to get a homogeneous catalyst ink. Next, 28 μL of the ink was drop-cast onto NGF substrate (mass loading = 1.1 mg cm^{-2}), and the as-obtained electrode was dried at room temperature before electrochemical measurements.

Acknowledgements

This work was supported by Foundation from Institute of Materials, CAEP (TCSQ2016306, TP03201802 and TP03201703).

Conflict of Interest

The authors declare no conflict of interest.

Keywords: hydrothermal synthesis · oxygen evolution reactions · nanosheet arrays · doped graphite foam · water splitting

[1] S. Y. Tee, K. Y. Win, W. S. Teo, L. D. Koh, S. Liu, C. P. Teng, M. Y. Han, *Adv. Sci.* **2017**, *4*, 1600337.
[2] M. Tahir, L. Pan, F. Idrees, X. Zhang, L. Wang, J. J. Zou, Z. L. Wang, *Nano Energy*, **2017**, *37*, 136–157.
[3] N. T. Suen, S. F. Hung, Q. Quan, N. Zhang, Y. J. Xu, H. M. Chen, *Chem. Soc. Rev.* **2017**, *46*, 337–365.
[4] B. M. Hunter, H. B. Gray, A. M. Muller, *Chem. Rev.* **2016**, *116*, 14120–14136.
[5] J. Kibsgaard, T. R. Hellstern, S. J. Choi, B. N. Reinecke, T. F. Jaramillo, *ChemElectroChem* **2017**, *4*, 2480–2485.
[6] A. Grimaud, A. Demortiere, M. Saubanere, W. Dachraoui, M. Duchamp, M. L. Doublet, J. M. Tarascon, *Nat. Energy* **2017**, *2*, 16189.
[7] S. Cherevko, S. Geiger, O. Kasian, N. Kulyk, J. P. Grote, A. Savan, B. R. Shrestha, S. Merzlikin, B. Breitbach, A. Ludwig, K. J. Mayrhofer, *Catal. Today* **2016**, *262*, 170–180.
[8] I. Roger, M. A. Shipman, M. D. Symes, *Nat. Rev. Chem.* **2017**, *1*, 0003.
[9] Y. P. Zhu, C. Guo, Y. Zheng, S. Z. Qiao, *Acc. Chem. Res.* **2017**, *50*, 915–923.
[10] Y. Yan, B. Y. Xia, B. Zhao, X. Wang, *J. Mater. Chem. A* **2016**, *4*, 17587–17603.
[11] J. R. Galan Mascaros, *Chemelectrochem*, **2015**, *2*, 37–50.
[12] D. Yan, Y. Li, J. Huo, R. Chen, L. Dai, S. Wang, *Adv. Mater.* **2017**, *29*, 1606459.
[13] J. P. Kumar, S. D. Giri, A. Sarkar, *Int. J. Hydrogen Energy* **2018**, *43*, 15639–15649.
[14] W. Zhou, X. F. Lu, J. J. Chen, T. Zhou, P. Q. Liao, M. Wu, G. R. Li, *ACS Appl. Mater. Interfaces* **2018**, *10*, 38906–38914.
[15] S. Li, Y. Wang, S. Peng, L. Zhang, A. M. Al-Enizi, H. Zhang, X. Sun, G. Zheng, *Adv. Energy Mater.* **2016**, *6*, 1501661.
[16] J. Deng, M. R. Nellist, M. B. Stevens, C. Dette, Y. Wang, S. W. Boettcher, *Nano Lett.* **2017**, *17*, 6922–6926.
[17] J. Dong, F. Q. Zhang, Y. Yang, Y. B. Zhang, H. He, X. Huang, X. Fan, X. M. Zhang, *Appl. Catal. B* **2019**, *243*, 693–702.
[18] X. Cheng, C. Lei, J. Yang, B. Yang, Z. Li, J. Lu, X. Zhang, L. Lei, Y. Hou, K. Ostrikov, *ChemElectroChem* **2018**, *5*, 3866–3872.
[19] F. Wang, Y. Zhu, W. Tian, X. Lv, H. Zhang, Z. Hu, Y. Zhang, J. Ji, W. Jiang, *J. Mater. Chem. A* **2018**, *6*, 10490–10496.
[20] J. Masa, C. Andronescu, H. Antoni, I. Sinev, S. Seisel, K. Elumeeva, S. Barwe, S. Marti-Sanchez, J. Arbiol, B. R. Cuenya, M. Muhler, W. Schuhmann, *ChemElectroChem* **2019**, *6*, 235–240.
[21] P. Li, H. C. Zeng, *J. Mater. Chem. A* **2018**, *6*, 2231–2238.
[22] S. Wang, J. Wu, J. Yin, Q. Hu, D. Geng, L. M. Liu, *ChemElectroChem* **2018**, *5*, 1357–1363.
[23] S. Zhuang, L. Wang, H. Hu, Y. Tang, Y. Chen, Y. Sun, H. Mo, X. Yang, P. Wan, Z. U. H. Khan, *ChemElectroChem* **2018**, *5*, 2577–2583.
[24] L. Yu, J. F. Yang, B. Y. Guan, Y. Lu, X. W. Lou, *Angew. Chem. Int. Ed.* **2018**, *57*, 172–176
[25] D. Zhou, Z. Cai, Y. Bi, W. Tian, M. Luo, Q. Zhang, Q. Zhang, Q. Xie, J. Wang, Y. Li, Y. Kuang, X. Duan, M. Bajdich, S. Siahrostami, X. Sun, *Nano Res.* **2018**, *11*, 1358–1368.

[26] R. Gao, D. P. Yan, *Adv. Energy Mater.* **2019**, 1900954.
[27] W. Ye, X. Fang, X. Chen, D. Yan, *Nanoscale* **2018**, *10*, 19484–19491.
[28] Z. Li, M. Shao, Q. Yang, Y. Tang, M. Wei, D. G. Evans, X. Duan, *Nano Energy* **2017**, *37*, 98–107.
[29] S. Yin, W. Tu, Y. Sheng, Y. Du, M. Kraft, A. Borgna, R. Xu, *Adv. Mater.* **2018**, *30*, 1705106.
[30] M. Arif, G. Yasin, M. Shakeel, M. Mushtaq, W. Ye, X. Fang, S. Ji, D. Yan, *Mater. Chem. Front.* **2019**, 3, 520–531.
[31] M. Arif, G. Yasin, M. Shakeel, X. Fang, R. Gao, S. Ji, D. Yan, *Chem. Asian J.* **2018**, *13*, 1045–1052.
[32] C. Deng, K. H. Wu, J. Scott, S. Zhu, R. Amal, D. W. Wang, *ChemElectroChem* **2018**, *5*, 732–736.
[33] A. Nadeema, V. M. Dhavale, S. Kurungot, *Nanoscale* **2017**, *9*, 12590–12600.
[34] L. Du, L. Luo, Z. Feng, M. Engelhard, X. Xie, B. Han, J. Sun, J. Zhang, G. Yin, C. Wang, Y. Wang, Y. Shao, *Nano Energy* **2017**, *39*, 245–252.
[35] C. Tang, H. S. Wang, H. F. Wang, Q. Zhang, G. L. Tian, J. Q. Nie, F. Wei, *Adv. Mater.* **2015**, *27*, 4516–4522.
[36] C. Tang, H. F. Wang, Q. Zhang, *Acc. Chem. Res.* 2018, 51, 881–889.
[37] C. Tang, L. Zhong, B. Zhang, H. F. Wang, Q. Zhang, *Adv. Mater.* **2018**, *30*, 1705110.
[38] W. Xu, Z. Lu, X. Sun, L. Jiang, X. Duan, *Acc. Chem. Res.* **2018**, *51*, 1590–1598.
[39] Y. Li, H. Zhang, M. Jiang, Q. Zhang, P. He, X. Sun, *Adv. Funct. Mater.* **2017**, *27*, 1702513.
[40] H. Xu, J. X. Feng, Y. X. Tong, G. R. Li, *ACS Catal.* **2017**, *7*, 986–991.
[41] C. Xiao, Y. Li, X. Lu, C. Zhao, *Adv. Funct. Mater.* **2016**, *26*, 3515–3523.
[42] Y. Li, L. Zhang, X. Xiang, D. P. Yan, F. Li, *J. Mater. Chem. A* **2014**, *2*, 13250–13258.
[43] Q. Yang, T. Li, Z. Lu, X. Sun, J. Liu, *Nanoscale* **2014**, *6*, 11789–11794.
[44] Z. Wang, L. Zhang, *ChemElectroChem* **2018**, *5*, 1153–1158.
[45] R. Gao, D. Yan, *Nano Res.* **2018**, *11*, 1883–1894.
[46] F. Wang, J. Zhao, W. Tian, Z. Hu, X. Lv, H. Zhang, H. Yue, Y. Zhang, J. Ji, W. Jiang, *RSC Adv.* **2019**, *9*, 1562–1569.
[47] R. Li, J. Xu, J. Ba, Y. Li, C. Liang, T. Tang, *Int. J. Hydrogen Energy* **2018**, *43*, 7956–7963.
[48] Z. Lu, Y. Li, X. Lei, J. Liu, X. Sun, *Mater. Horiz.* **2015**, *2*, 294–298.
[49] R. Li, M. Zhang, Y. Li, J. Chen, B. Yao, M. Yu, G. Shi, *Phys. Chem. Chem. Phys.* **2016**, *18*, 11104–11110.
[50] H. Wang, T. Maiyalagan, X. Wang, *ACS Catal.* **2012**, *2*, 781–794.
[51] J. Ji, J. Liu, L. Lai, X. Zhao, Y. Zhen, J. Lin, Y. Zhu, H. Ji, Li. Zhang, R. Ruoff, *ACS Nano*, **2015**, *9*, 8609–8616.
[52] D. Zhou, Z. Cai, X. Lei, W. Tian, Y. Bi, Y. Jia, N. Han, T. Gao, Q. Zhang, Y. Kuang, J. Pan, X. Sun, X. Duan, *Adv. Energy Mater.* **2018**, *8*, 1701905.
[53] X. Yu, M. Zhang, W. Yuan, G. Shi, *J. Mater. Chem. A* **2015**, *3*, 6921–6928.
[54] D. M. Oscar, L. Y. Isis, T. M. K. Marc, C. V. Federico, *ACS Catal.* **2015**, *5*, 5380–5387.
[55] S. Eigler, S. Grimm, F. Hof, A. Hirsch, *J. Mater. Chem. A* **2013**, *1*, 11559–11562.
[56] G. Zhang, Y. Li, Y. Zhou, F. Yang, *ChemElectroChem* **2016**, *3*, 1927–1936.
[57] Y. Sun, C. Liu, L. Zhang, P. Wan, S. Zhuang, Y. Tang, Y. Chen, J. Pan, *ChemElectroChem* **2017**, *4*, 1044–1050.
[58] Y. Ni, L. Yao, Y. Wang, B. Liu, M. Cao, C. Hu, *Nanoscale* **2017**, *9*, 11596–11604.
[59] G. Wang, D. Zheng, D. Liu, J. Harris, J. Si, T. Ding, D. Qu, *Electrochim. Acta* **2017**, *247*, 722–729.
[60] D. Friebel, M. W. Louie, M. Bajdich, K. E. Sanwald, Y. Cai, A. M. Wise, M. J. Cheng, D. Sokaras, T. C. Weng, R. Alonso Mori, R. C. Davis, J. R. Bargar, J. K. Norskov, A. Nilsson, A. T. Bell, *J. Am. Chem. Soc.* **2015**, *137*, 1305–1313.
[61] M. W. Louie, A. T. Bell, *J. Am. Chem. Soc.* **2013**, *135*, 12329–12337.
[62] X. Yu, M. Zhang, J. Chen, Y. Li, G. Shi, *Adv. Energy Mater.* **2016**, *6*, 1501492.

Manuscript received: June 1, 2019
Revised manuscript received: June 27, 2019